# Shear Stress Behavior on Complex Rough Surfaces

J.A. Gillies and W.G. Nickling

## 1. Introduction

Computation of shear stress from time averaged wind velocity profiles is common practice in aeolian research because the shear stress created by the wind and exerted on the surface is an important control on sediment entrainment and transport. It is generally accepted that the shear stress exerted upon the surface can be determined from application of the Prandtl equation (Prandtl, 1932):

$$\frac{u_z}{u_*} = \frac{1}{k} \ln \frac{z}{z_0} \tag{1}$$

where  $u_z$ = wind velocity at height $z$ (m s$^{-1}$)
   $u_*$= wind friction velocity (m s$^{-1}$)
   $k$ = von Karman's constant ($\sim$ 0.4)
   $z$ = height above the surface (m)
   $z_0$= roughness length (m)

The boundary shear stress is related to the wind friction velocity through the expression:

$$\boldsymbol{t}_0 = r\, u_*^2 \tag{2}$$

where  $\boldsymbol{t}_0$ = boundary shear stress (N m$^{-2}$)
   $\boldsymbol{r}$ = air density (kg m$^{-3}$)

The "*law of the wall*", as embodied in Equation 1, ignores the more transitory effects of turbulence that are inherent in the flow, and influenced by the bed roughness (Raupach *et al*., 1980; Krogstad *et al*., 1992). These important characteristics of turbulence include the "burst-sweep" cycle (Rao *et al*., 1970) and the dynamic effect of instantaneous changes in shear stress caused by rapidly changing fluid velocities and directions. Recently, researchers examining saltation dynamics have shown the importance of these turbulent phenomena in aeolian sand transport (Butterfield, 1991, 1993; Hardisty, 1993). The effects of these intermittent processes and the resultant stresses they create have not been directly measured on surfaces of different roughness dimensions.

The purpose of this paper is to examine the surface shear stress behaviour for surfaces of different roughness in a wind tunnel and to offer an explanation for the observed behaviour in light of recent advances in understanding turbulent processes.

## 2. Instrumentation

For this research a newly designed, relatively low cost, drag plate was constructed to measure the surface shearing stress on representative surface samples in a wind tunnel boundary layer. Figure 1 shows a schematic of the mechanics of the drag plate. The drag plate surface dimensions are 0.3 ´ 1.0 m, with the long axis positioned parallel to the wind tunnel working section. Basically, the form is a box construction that can deform to the right or left of the perpendicular position along the wind tunnel axis. The box is restrained from movement by joining one of the lever frames to a load cell with a small length of threaded rod. The load cell is held on a platform fixed to the lower base. The drag plate has four levelling feet incorporated into the base plate to ensure that the top plate is balanced

evenly in both axes, eliminating, as much as possible, any torque in the shafts and lever arms. The system must also be level to eliminate bluff-body drag effects acting on a tilted surface.

Displacement of the top plate relative to the fixed bottom base is transferred via the lever arm to the threaded rod and load cell. The load cell produces a voltage change that is proportional to the displacement distance. When the top of the drag plate is displaced horizontally due to the wind drag, the spring constant ($1.45 \times 10^4$ N m$^{-1}$) acts to restore equilibrium in the system.

The electronic components of the drag plate system include a load cell (Transducer Techniques, model GS-150), a 12 volt DC power supply and signal conditioner (Gould Bridge amplifier, model 134312), and an analogue to digital data acquisition board (Kiethly-Metrabyte, model DAS 1401) in a personal computer.

Calibration of the system within the stress range of 0 to 1.5 N m$^{-2}$ was carried out using weights hanging over a precision bearing and pulley system to convert their action to a horizontal pull or push on the drag plate. Force per unit area is obtained by division with the two dimensional plan area of the top plate (0.3 m$^2$). No significant departures from linearity were apparent (Figure 2) in the relationship between applied weight and voltage output. The coefficient of determination ($r^2$) calculated from the regression analysis for the data represented in Figure 2 is 0.9997 with a standard error of $\pm 4.13 \times 10^{-4}$ N. The calibration procedure was done *in situ* and repeated after each test run. Based on the mass of the top plate and the spring constant of the load cell the natural frequency of the system can be calculated and was determined to be 8 Hz. The data acquisition system operated at 1 Hz. It is important to note that neither the period nor the frequency depends upon the amplitude (maximum displacement) of the vibrating body. They depend only on the spring constant and the mass of the vibrating body (Tippens, 1978) which was equalised for each test surface by adding mass to the underside of the top plate.



| | |
|---|---|
| 1) Precision Bearings | 5) Calibration Mechanism |
| 2) Lever Arm | 6) Test Surface |
| 3) Threaded Rod | 7) Dash Pot |
| 4) Load Cell | 8) Levelling Feet |
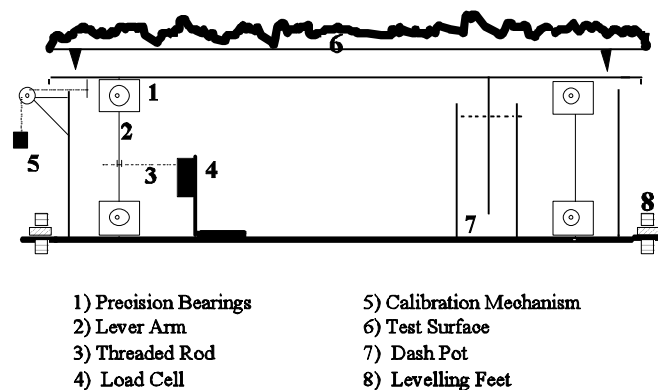
**Figure 1**. Schematic diagram of the drag plate mechanics. The test surface is fixed to a board that is held in place on the top plate by machine screws.
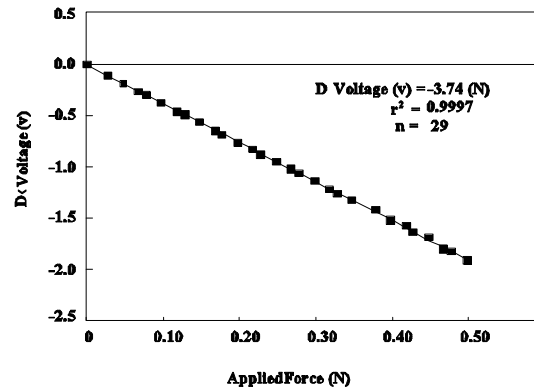
**Figure 2**.  A full calibration curve defining the response of the load cell in the drag plate to an applied force (a hanging weight).

Wind velocity and surface shear stress measurements were made in a straight line, 12 m long 0.75 m high suction type wind tunnel.  The drag plate was approximately 10.5 m from the inlet.  The wind profile over the drag plate was measured with an array of 24 Pitot tubes that extend 0.13 m into the air stream, 0.90 m from the leading edge of the drag plate.  Additional wind velocity profiles were measured at 7.2 m, 8.5 m, and 9.8 m from the inlet for each test surface and freestream velocity.  A scanning valve controlled by an A/D board connected to a sensitive pressure transducer (accuracy 0.25% of FSO at 0-5" W.C.D.) selectively samples the dynamic air pressure in each tube for a 2 s period, so that a full scan of the wind velocity profile was completed every 48 s.  The first 0.5 s of each 2 s sampling interval, representing the time required for the pressure in the Pitot tube lines to come into equilibrium, was ignored.

A laser scanner was used to measure the surface roughness (Gillies, 1994).  The scanner was based upon an original design by Huang *et al*. (1988).  The scanner consists of a low-powered HeNe laser, mounted on an *X-Y* traversing frame, that projects a parallel beam onto the soil surface (Figure 3).  The reflected laser light from the soil surface is focused by a conventional 50 mm camera lens onto a linear photo-diode array mounted at the back of a camera.  The high intensity of the reflected laser spot produces a strong output from the diode array.  The optical transducer used in the scanner is a monolithic self-scanning linear 512 element photodiode array (EG&G Reticon, model RL0512GAG).  According to Huang and Bradford (1992), a 512-element array will give a resolution of approximately 0.1 % of the measurement range.  The array is positioned within the camera body such that the sensing elements lie along the centreline of the lens in the perpendicular axis and at the plane at which the film would lie.

The relative position of the laser image along the photodiode array is detected electronically in three modes: an analogue voltage output, transistor-transistor logic (TTL) and visually on an oscilloscope display.  The TTL digital output of the photodiode is sampled by a digital input/output (DI/O) board (Computer Boards Inc., model CI0-DI024) in a Personal Computer.  Detection of the diode receiving the most light energy is accomplished by circuitry comprised of a voltage comparator with a threshold detector.  The photo-diode with the highest output on the array can be related to the surface elevation by trigonometric relationships (Huang *et al*., 1988).  Horizontal resolution of the scanner is 1 mm with a vertical resolution of ±0.1 mm.
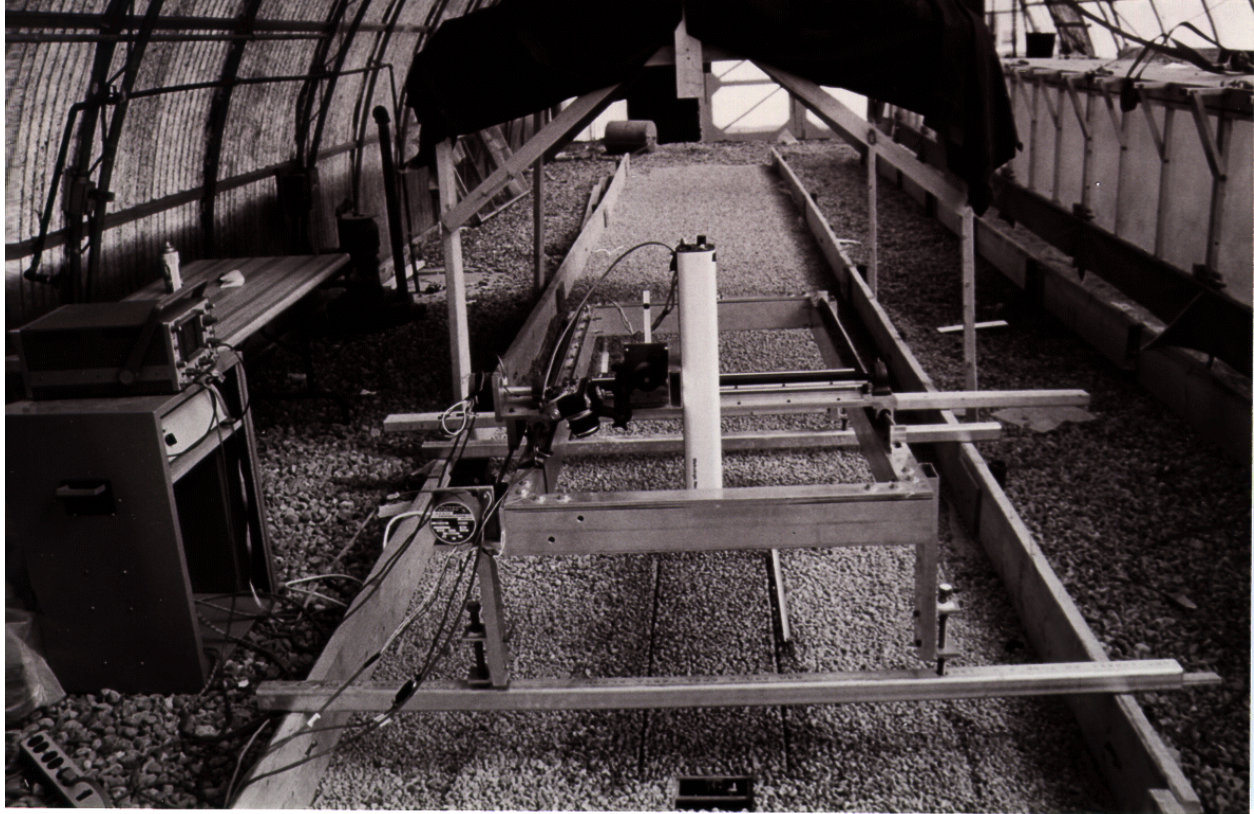
**Figure 3**. The laser scanner used to determine the elevation distribution of the test surfaces. The installed drag plate is also in view below the scanner. The back cover has been removed to show the access to the calibration system.


### 3. Experimental Procedure

Quarried and screened gravels of nominal sizes 25.4, 12.7, and 6.4 mm were used to create the complex rough surfaces. The material was placed into a crib of dimensions 13´1.75´0.30 m to a depth of 0.10 m. Representative samples of the test surfaces were affixed to the top plate of the drag plate by gluing the test material to a board the same size as the plate (1.0 ´ 0.3 m). To achieve a representative surface configuration, the material was laid down on the board several grain thicknesses deep, and then set in place by aerosol spray glue. The board with the fixed gravel surface was then placed on the top plate of the drag plate and attached with machine screws. Once the test surface was prepared, the drag plate and wind velocity measuring instrumentation were installed, and the wind tunnel was placed over the surface.

For each test surface six different velocities were used to characterize the relationship between profile-derived shear stress and the shear stress determined from the drag plate. Each individual test lasted for 960 seconds and was replicated 5 times. The 20 wind profiles measured during a test were

subsequently averaged to remove the effects of any unsteady flow in the tunnel that may be apparent if only a single profile had been used.

Upon completion of a test series the gravel surface was scanned using the laser profiler in three different locations upwind of the drag plate as well as the drag plate itself. Surface elevation measurements were taken every 1 mm for a 1 m long transect. A total of 55 transects with 50 mm between scan lines were taken for each surface roughness sample. Each surface roughness sample consisted of approximately 50,000 $x$, $y$, and $z$ co-ordinate points within an area of 0.3 m$^2$. A marker for the bottom Pitot tube was included in the scan that allowed the heights above the surface at which the wind velocity was measured to be precisely determined. Since the Pitot tube rake rested on the topmost surface roughness elements, the position of the bottom tube would be different between each surface, which does not allow for measurement of the wind velocity at precisely the same heights between surfaces. The height of the bottom Pitot tube varied by a few millimetres between the three surfaces.

## 4. Results

The surface elevation characteristics for each test surface, including standard statistical measures of the mean and standard deviation of elevation were calculated for each of the laser scanner collected data sets using the method of moments (Krumbein and Pettijohn, 1988). Before analysis of the elevation data, the data were detrended to remove any slope component that may have been a function of a systematic levelling error in the laser scanner frame. Figure 4 shows histograms of the elevation distribution for the three surfaces affixed to the drag plate. The statistical measures for the elevation data acquired at all the sampling positions, for each of the three surfaces, are given in Table 1.

Figure 5 illustrates the general form of the time averaged wind velocity profiles measured in the wind tunnel, over the drag plate, for each of the gravel beds for the range of wind velocities used. The basic form of the wind velocity profiles illustrated in Figure 5 were typical of the wind tunnel tests at all measurement positions. On semi-logarithmic axes the profiles are characterized by an upper straight line segment that begins at some point above the surface extending upwards through the sampling height. The upper straight line segments appeared to conform to the characteristic form of the *law of the wall* (Prandtl, 1932).
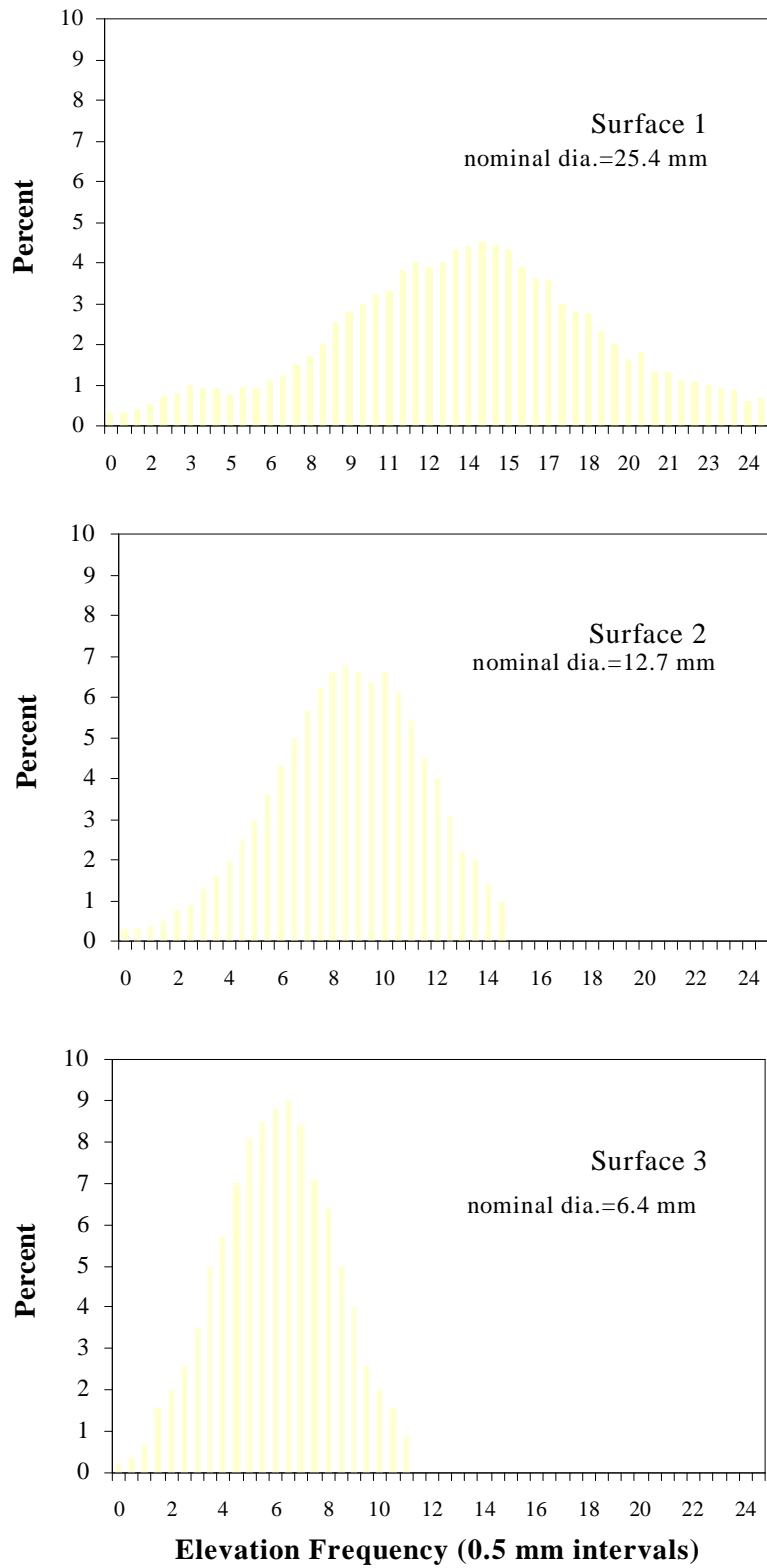
**Figure 4**. The elevation distribution of the three surfaces affixed to the drag plate as determined with the laser scanner.

| Surface and Position | Mean (mm) | Standard Deviation (mm) | Mode (mm) | Skewness |
|---|---|---|---|---|
| 1, A[1] | 13.4 | 4.9 | 14.8 | -0.18 |
| 1, B[2] | 13.6 | 4.4 | 14.0 | -0.66 |
| 1, C[3] | 12.9 | 4.0 | 15.8 | -0.65 |
| 1, D[4] | 13.0 | 4.0 | 14.5 | -.38 |
| 2, A | 8.8 | 2.9 | 8.5 | -0.41 |
| 2, B | 10.1 | 3.7 | 9.5 | 0.16 |
| 2, C | 12.6 | 5.0 | 13.5 | -0.18 |
| 2, D | 12.3 | 4.6 | 14.5 | -0.48 |
| 3, A | 6.2 | 2.2 | 6.5 | -0.14 |
| 3, B | 7.7 | 3.4 | 7.5 | 0.06 |
| 3, C | 9.0 | 3.3 | 9.5 | -0.15 |
| 3, D | 7.3 | 2.7 | 7.5 | -0.07 |

[1] The drag plate surface, 11.5 m from the wind tunnel entrance.
[2] Measurement taken 9.8 m from wind tunnel entrance.
[3] Measurement taken 8.5 m from wind tunnel entrance.
[4] Measurement taken 7.2 m from wind tunnel entrance.

**Table 1**.  The surface elevation statistics calculated by the method of moments from measurements obtained with the laser scanner.

Close to the surface, below the upper straight segments, the slope of the velocity profiles depart from the semi-logarithmic form, and decreases much more rapidly with height within the last few millimetres above the tops of the roughness elements.  This form of velocity profile has also been observed over rough surfaces in other wind tunnel studies (Raupach *et al*., 1980; Krogstad *et al*., 1992). The zone close to the bed, below the semi-logarithmic profile, is termed the *roughness sublayer* (Raupach *et al*., 1980) in which wakes generated by the roughness elements complicate the flow and the vertical profile form is dependent on surface defined length scales.  Quantitative description of this layer is lacking due to the complexity of the flow characteristics, difficulty in measurement and the uncertainty in defining the appropriate surface scales (Raupach *et al*., 1980).

Using the *law of the wall* as a basis for determining the wind borne shear stress requires identification of the regions which correspond to the inertial and roughness sublayers because the *law of the wall* only applies within the inertial sublayer (Raupach *et al*., 1980).  The height of the roughness sublayer was estimated from visual examination of the wind velocity profile plots for each test by noting at which Pitot tube the profile seemed to distinctly depart from the apparent log-linear form (Figure 5).
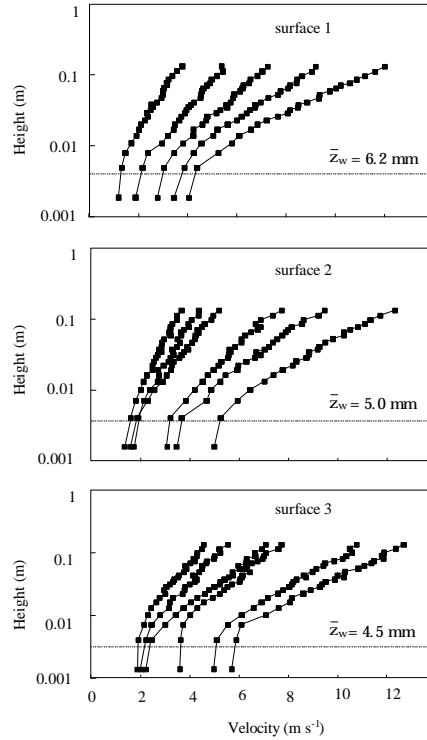
**Figure 5**. Representative wind profiles measured over the test surfaces above the drag plate. The dotted line demarcates the average height of the roughness sublayer ($\bar{z}_w$).

This can only give an approximation to the position of the roughness sublayer as the increments of height measurement for the velocity profile are tied to the Pitot tube spacing. The average height of the discontinuity in the profiles as determined by the position of the Pitot tubes for each surface and test position were: surface *1*, 6.2 mm; surface *2*, 5.0 mm; and surface *3*, 4.5 mm, in order of decreasing geometric roughness.

The *law of the wall* suggests that wind velocity profiles within the inertial sub-layer are characterized by a logarithmic increase of wind velocity with increasing height above the boundary and, according to theory, may be described by the relationship defined by the Prandtl equation (Equation 1). A least squares regression was performed on only the data points above the estimated roughness layer to assess the fit of the wind velocity profile to the Prandtl model and to determine the friction velocity, $u_*$ (m s$^{-1}$). The coefficient of determination ($\rho^2$) for the velocity and *ln* height relationship ranged between 0.934 to 0.996 with an average value of 0.980 for the entire series of tests. The profiles identified as the inertial sublayer were quite well described by the Prandtl equation in terms of the statistical fit determined by least squares regression.

Friction velocities calculated from the regression procedure for each test were found to cover a range from approximately $u_*$=0.2 to 1.0 m s$^{-1}$. This range is comparable to friction velocities measured in the atmosphere (Nickling and Gillies, 1993) as well as for other wind tunnel studies (McKenna-Neuman and Nickling, 1994; Williams *et al*., 1994). The friction velocity was also converted to a shear stress ($t_0$) using Equation 2 in order to make a direct comparison with the surface shear stress ($t_s$) measured with the drag plate.

8

The surface shear stress measured directly for each of the gravel beds covered a range from approximately 0.1 to 1.0 N m$^{-2}$ with the roughest test surface having higher values of up to 1.5 N m$^{-2}$. These values are within the range reported by Bradley (1968) who used a larger drag plate in the field with natural winds. The relationship between the time averaged surface shear stress, $t_0$, and profile shearing stress, $t_p$, observed for the three different surface roughness configurations tested in this research are illustrated in Figure 6. The best fit least squares regression lines are also shown for each data set. The relationships illustrated in Figure 6 are very strong, and are significant at the 0.01 level for all three surface data sets, indicating that surface shearing stress was highly correlated to the shearing stress in the fluid. However, it is evident from Figure 6 that the relationship between the profile based shear stress and the shear stress measured directly with the drag plate is not 1:1 for any of the surfaces tested.

For surface *1*, the roughest surface, the shear stress measured with the drag plate is on average 1.59 times greater than the calculated wind profile shear stress ($t_0$). For surface 2, this ratio decreased to 1.42 and for the least rough surface (surface 3) the ratio decreased to 0.86 after removing four data points from the wind speed profile measurements taken at 7.2 m from the wind tunnel inlet. These four data point sat apart from the general trend in the data with $t_s$ values that appear to be too low in relation to the rest of the runs. This may have resulted from the lodging of a small stone in the annular gap that restricted the free movement of the drag plate resulting in lower $t_s$ values.

Based on the analysis of the mechanics of the drag plate and acceptance of previous results for determining friction velocity with a similar Pitot tube rake and the same pressure transducer (McKenna-Neuman and Nickling, 1994; Nickling and McKenna-Neuman, 1994) it is unlikely that the differences in the measured shear stress values would be in error by as much as 40%. For the gravel surface with the least elevational range (surface *3*), the percent difference between the directly measured drag plate shear stress and the wind profile derived shear stress, taking into account the potential sources of error, was probably not significantly different from a one to one relationship.

During the wind tunnel tests, the drag plate was observed to oscillate (backwards and forwards) with short periods of intense movement followed by more subtle movement. Some important observations of the behaviour of the instantaneous shear stress can be gained by examining the variability in the shear stress as quantified by its standard deviation and also by examining the distribution of stress events during a test.

Figure 7 illustrates the changes in surface shear stress through time as measured by the drag plate for one series of six increasing freestream velocities for surface *3*. Figure 7 shows that concomitant with an increase in the average surface shear stress with increasing wind velocity, there was an increase in the standard deviation ($s_{ts}$). This type of pattern was observed for all the tests and may reflect an increase in the turbulent burst sweep cycle that Raupach (1981) found to scale with increased roughness. In order to quantify the variability in terms of both the flow characteristics and a measure of roughness, bed Reynolds numbers ($Re_b$) were calculated for each test and compared to the standard deviation of the bed shear stress. The $Re_b$ is defined by:

$$\mathrm{Re}_b = \frac{\rho_f u_* H}{\mu} \tag{3}$$

where $r_f$ = fluid density (kg m$^{-3}$)

$u_*$ = friction velocity (m s$^{-1}$)

$H$ = range of height associated with the roughness elements (m)

$m$ = fluid viscosity (N s m$^{-2}$).
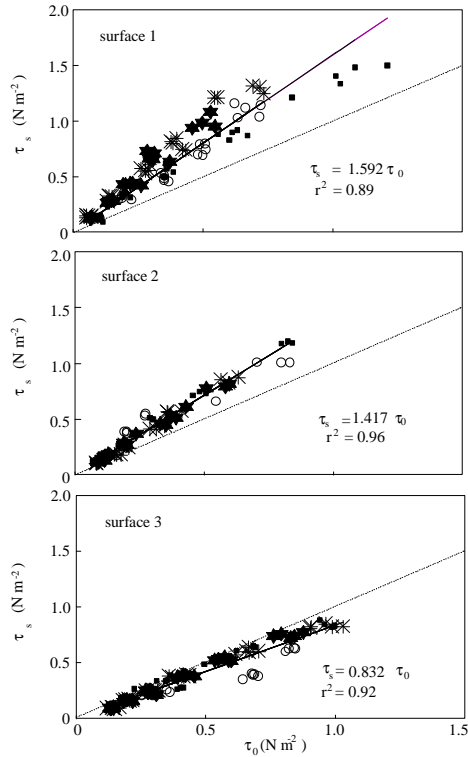


**Figure 6**. The relationship between the shear stress measured on the surface ($t_s$) with the drag plate and indirectly from the wind velocity profiles ($t_0$) for the three test surfaces. Different symbols represent the data for each of the four positions at which $t_0$ was calculated. The dotted line indicates the theoretical 1:1 relationship.

The friction velocities used in the bed Reynolds number calculations were obtained from the wind velocity profiles. The calculated $Re_b$ values for the three gravel surfaces were all greater than 60 indicating the flow was dynamically rough (Middleton and Southard, 1984). The relationships between $Re_b$ and the standard deviation of $t_s$ for each of the surfaces, combining all the tests, are illustrated in Figure 8. The data indicate a very strong linear relationship, significant at the 0.01 confidence level between $Re_b$ and the standard deviation of $t_s$ for each of the test surfaces. However, the slopes defining the best fit lines are different, which suggests that the variability in shear stress is both a function of increasing inertial forces in the wind, as defined by an increasing $Re_b$, as well as a function of surface roughness. The variability in shear stress increased more rapidly with increasing $Re_b$ for surface *1* that had a greater elevational range than the other two surfaces. As elevational range diminished between surfaces *2* and *3*, the variability in shear stress with increasing $Re_b$ also decreased.

10
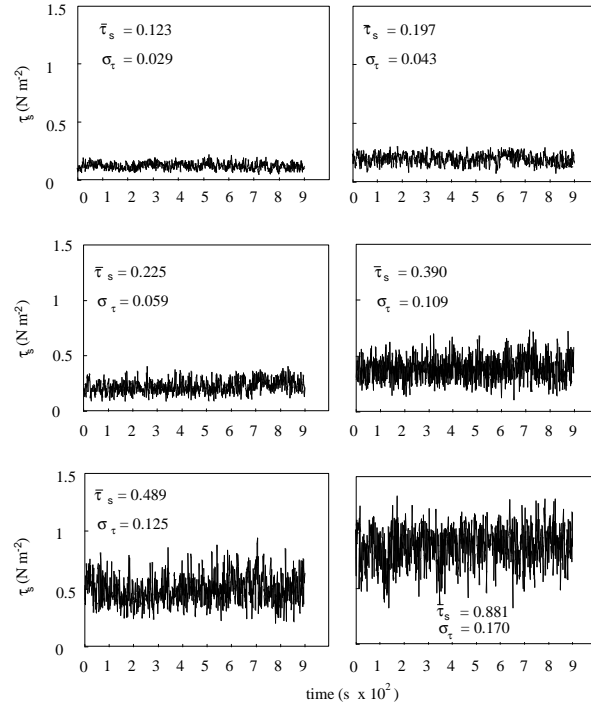
**Figure 7**. The changes in surface shear stress through time as measured by the drag plate for one series of six increasing freestream velocities for surface *3*.
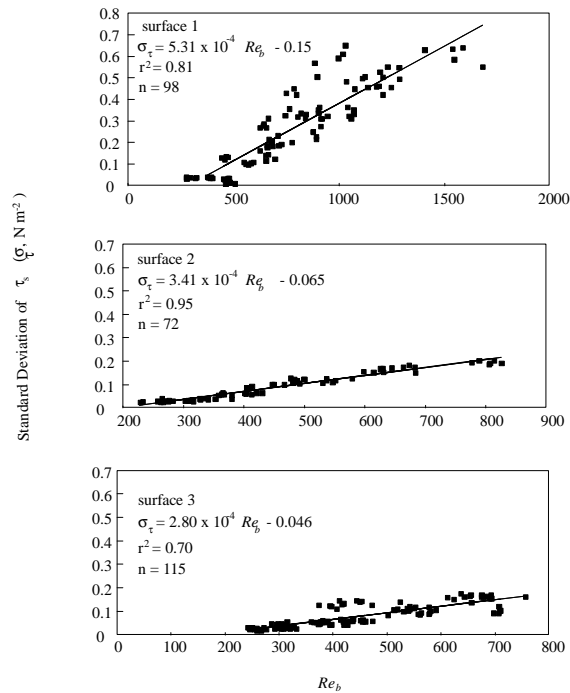


**Figure 8**. The relationship between standard deviation of $t_s$ and $Re_b$ for each of the test surfaces. The data are plotted at different scales to illustrate the form of the individual relationships that would be less apparent if plotted at the same scale.

These observed relationships suggest that a physical mechanism associated with increasing roughness, was in part responsible for the variability in surface shear stress.

In addition to the noted increase in the variability of $t_s$ with increasing $Re_b$, the actual distribution of instantaneous stress also appears to change with $Re_b$. Figure 9 illustrates the changes in the skewness of the shear stress distribution for increasing $Re_b$ associated with the test surfaces. For surfaces *2* and *3* there was a trend for the distribution of shear stress to become more negatively skewed with increasing $Re_b$. This was most clearly shown for surface *3*. Surface *2* showed the same trend, but not quite so strongly. It would seem that for these two surfaces an increase in $Re_b$ created more sustained, higher stress events that were displacing the drag plate. The skewness and $Re_b$ data for the roughest surface (Figure 9a) did not show the same relationship that was found for the other surfaces. The only apparent trend was for the distribution of shear stress to become more normally distributed with increasing $Re_b$. The apparent change in the trend for surface *1* may reflect the higher overall variability in shear stress or results from a mechanical effect whereby the drag plate cannot respond appropriately to the distribution of the stress events when they become sufficiently large. After the plate was moved forward (in the direction of the wind) by a large stress event, it tries to recover its original position under the restoring force of the spring constant. With large forward stresses, the backwards restoration movement will be the greatest, which may possibly allow enough inertia to be gained to effectively create an under response to the next forward directed stress. This response pattern would mask the effect of the higher frequency stress events and effectively normalise the distribution. This normalisation of stress events at high $Re_b$ would also account for the apparent downward shift in the data points for the highest $t_s$ values in Figure 4a (surface *1*). In this case the more normal distribution of stress measurements results in a lower mean value than would result from a distribution that is negatively skewed, which may be the reason why these points sit slightly below the expected relationship.

## 5. Discussion

The upper portion of the wind velocity profiles measured over the test surfaces were well defined by the logarithmic form with a gradient closely approximated by $u_*/k$, which has been observed for other wind tunnel boundary layers (Raupach *et al.*, 1991). As well, a distinct break in slope close to the surface was observed where the streamwise velocity decreased very rapidly. According to Raupach *et al.* (1991), this is expected and defines the roughness sublayer ($z_w$) which is a zone close to the bed, characterised by flow inhomogeneities caused by interacting wakes shed from the roughness elements. Laboratory studies over three dimensional roughness have found that $z_w$ is between $2h$ and $5h$. Raupach *et al.* (1980) also suggested that the height is influenced by a lateral or transverse element dimension described by:

$$z_w = 1.5 \, l + h \tag{4}$$

where   $h$ = element height mm
         $l$ = element breadth (mm).

Assuming that $z_w$ is between $2h$ and $5h$ of the 95 percentile of height, $z_w$ should be between 38 and 95 mm for the roughest surface. Using the mean grain size diameters as the $l$, and the mean elevation as $h$, the heights of the roughness sublayers predicted from Equation 4 would have been approximately 27.6, 20.4 and 11.8 mm for surfaces *1*, *2*, and *3*, respectively. Even with a generous allowance for curvature, it does not seem evident from the wind velocity profile data that the roughness sublayer extended to these heights for these surfaces.
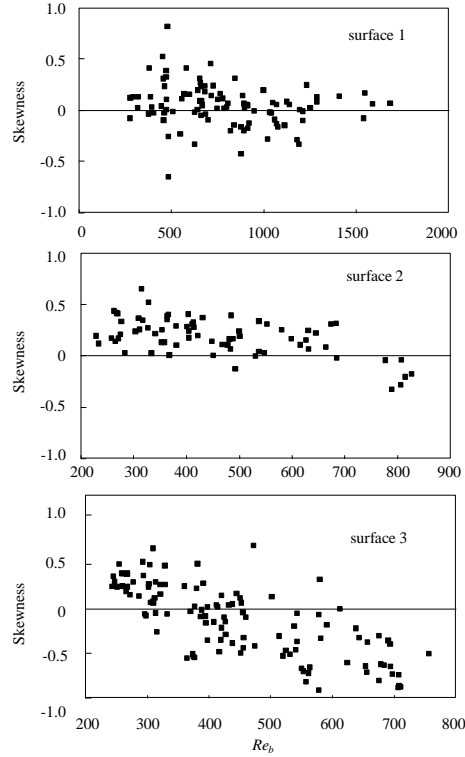
**Figure 9**. The relationship between the skewness of the shear stress distribution and $Re_b$ for each of the test surfaces.

The shallowness of the roughness layers is thought to result from the close packed arrangement of the gravels which is not taken into account in two dimensional models and may result from skimming type flow as described by Lee and Soliman (1977). The effect of element density has been noted by Raupach *et al*. (1980), Garratt (1980) and Wolfe (1993) to reduce the height of $z_w$. The density effect is related to the wake diffusion effect described by Raupach *et al*. (1980) which is enhanced by a more open structure or more sparsely distributed roughness elements. A second consideration that may explain the thin roughness sublayers found in this study is a form effect working in combination with the close packed structure. The primary roughness element type used in many of the previously cited studies were cylinders that favour the development of large vortices that are purely a function of their form. Iversen *et al*. (1991) found that cylinders shed vortices in the near wake region, but also for considerable distance downwind compared to block-like roughness. The key form parameter in the cylinder is the flat upper surface and the upwind curved surface of the sidewall that favours vortex formation on the lee sides (Iversen *et al*., 1991). However, the form of the gravel particles used for the two roughest beds, in the present study, are more streamlined and as a result, may shed smaller and less vigorous eddies that do not effect the velocity field as far above the surface as do cylinders. Consequently, $z_w$ may not scale to the same height for the gravel surfaces. In general, the wind velocity profiles measured in this research seem to be well represented by the inertial sublayer (*ISL*) and roughness sublayer *RSL* model (Raupach *et al*., 1991). Although there is some discrepancy in the magnitude of the *RSL* with respect to previous work, this may be explained, at least to some extent, by differences in the roughness concentration and the roughness form.

13

Traditional boundary layer theory defines the relationship between the shear stress in the fluid and the shear stress on the surface by Equation (2). However, this relationship has been found to be in disagreement with the data collected in this study as well as several others, notably Mulhearn and Finnigan (1978). That study also utilised a drag plate to measure directly the surface shear stress on randomly distributed gravel ($D = 14.5$ mm). Mulhearn and Finnigan (1978) found that the shear stress measured directly with the drag plate was 67% higher than the stress in the wind determined by eddy correlation methods using hot wire anemometry. The results of Mulhearn and Finnigan (1978) are very similar to the stress deficit relationship between the bed and profile shear stress found in this research for the roughest gravel surface. The gravel used by Mulhearn and Finnigan (1978) corresponds in height to approximately the 65 percentile of elevation distribution of test surface *1* (14.7 mm).

According to the arguments of Raupach *et al*. (1991) and the results of Krogstad *et al*. (1992), although the velocity profiles above the roughness may appear to show a shear stress deficit, in reality this can not occur if an inertial sublayer exists. If this is so, then reasons must be found for the increased shear stress measured with the drag plate, or conversely, the profile deficit must be explained.

Mulhearn and Finnigan (1978) proposed that the difference in stress measurements could be explained by the spatial scale of the mean flow variations. They found that close to a rough surface, there was considerable variation in surface shear stress and mean velocity, and the horizontal scale of these variations was large. This horizontal inhomogeneity in the near surface velocity field was also confirmed by Raupach *et al*. (1980) for a rough surface composed of small cylinders of height 6 mm with diameter 6 mm. No direct stress measurements were taken in that study. They found spatial periodicities in both the horizontal and vertical velocity components close to the roughness elements and zones in the element lees marked by sharp peaks in the horizontal profile and pronounced downward flow, with upflow occurring between elements.

Raupach *et al*. (1980) also distinguish a second purely mechanical influence on the wind field close to the roughness which they identify as wake diffusion. In this process vertically directed vorticity in the mean shear flow is transferred to streamwise directed vorticity, concentrated in the limbs of horseshoe vortices on the lee sides of roughness elements. These vortices draw high velocity fluid into the central wake region (Raupach *et al.*, 1980). In an irregular surface composed of different roughness element sizes, shapes and positions, some of the shed vortices should also interact directly with elements in the downstream position, perhaps adding to the positive pressure at the next obstacle front and thus increasing the drag. For a three dimensional roughness element the limit of the far wake region is approximately 5*h*, where *h* is element height (Taylor, 1988). This streamwise vortical component acting in the zone near the tops of the elements may account for some of the additional stress measured with the drag plate. In effect, this is not a horizontal shearing stress, but a bluff body force that acts on the upwind face of elements.

The bluff body force relationship in its simplest form is:

$$F_D = 0.5\ C_D\ \mathbf{r}_f A\ V^2 \tag{5}$$

where  $F_D$ = the force of drag ( )
  $C_D$ = drag coefficient
  $\mathbf{r}_f$ = fluid density (kg m$^{-3}$)
  $A$ = frontal area (m$^2$)
  $V$ = velocity (m s$^{-1}$)

This simple representation of a freestream condition will be much more complicated within the turbulent fluid environment amongst the roughness elements (Raupach *et al.*, 1986), and a representative model of the force interactions has not been worked out. However, some of the basic physical principles should still apply. The force that is generated by forms that are positioned normal to the flow would locally be much higher than the horizontal shearing force of the wind. The roughest surfaces with the greatest amount of irregular protuberances projecting into the flow may have a higher proportion of stress force attributed to bluff body interaction with the dominant horizontal flow. As elevational variation declines, the chances of bluff body interaction should decrease as a function of several scaling properties. There will be a reduction in the surface area of individual elements ($A$) which reduces the magnitude of $F_D$ even holding all other factors in Equation 5 the same. Also, the flow will become more uniform and the detailed flow behind individual elements will be of only very localised importance, which should raise the overall importance of the horizontal shearing stress in relation to any additional bluff body drag forces.

The presence of a stress surplus on the drag plate compared to the wind shear stress may also be attributed to the properties of the turbulent flow acting upon it. A large element projecting into the flow would be a source of bluff body drag in addition to the horizontal shear stress, even in laminar flow. With the addition of turbulence there is a completely different mechanism for bringing momentum in the form of coherent high velocity vortices, to the surface which are a fundamental part of the turbulent flow and are identified as sweeps (Rao *et al.*, 1970). The sweep events may also provide some of the additional stress that appears as a surplus in the drag plate measurements. In this research, the 1 Hz shear stress measurements from the drag plate provide an indication of the nature of the turbulent shear flow close to the rough test surfaces. From analysis of the variability in the shear stress, it would appear that in all three test surfaces the system became much more energetic as the wind shear increased. It was also observed that the magnitude of the variability in the shear stress measurements was linked with the roughness scale. This increase in shear stress variability was most likely a result of increased turbulence intensity close to the rough surfaces. This follows Raupach (1981) who found that the relative magnitude of the sweep component ($u\mathcal{C} > 0$, $v\mathcal{C} < 0$) increases both with surface roughness and with the proximity to the surface. According to Raupach (1981), this sweep dominated region delineates the roughness sublayer. The data of Krogstad *et al.* (1992) indicated that not only are burst and sweep events stronger and more frequent on rough wall surfaces in comparison to smooth surfaces, but that their frequency of occurrence is nearly twice as large for rough versus smooth wall. Krogstad *et al.* (1992) also speculated that the vertical velocity spectrum may scale with roughness.

The drag plate data clearly indicate this roughness effect. Increasing surface roughness was related to elevated levels of turbulence intensity as measured by the increase in standard deviation of the instantaneous shear stress with increasing $Re_b$. A second trend in the shear stress data collected for surfaces *2* and *3* was the distinct change to a more negatively skewed frequency distribution as the friction velocity increased (Figure 9). This suggests that there was an increase in the frequency of relatively larger instantaneous stress events as the friction velocity increased which could be indicative of an increasing downward directed flow event or sweep. A second process may also be responsible for the increased activity that is related to the flow itself. According to Levi (1983), the periodicity of the stress generating events scales with a velocity term and may follow a universal Strouhal law. In this view, the frequency of the burst sweep cycle should scale with the boundary layer thickness as well as the free stream velocity.

With the increased frequency and increased magnitude of sweep events occurring on the rougher surfaces, additional velocity components that are not horizontal may play a role in increasing the stress measurements on the drag plate. Raupach *et al*. (1986) examined the higher velocity moments of the horizontal and vertical velocity and concluded that the solid boundary deflects downward moving gusts (or sweeps) into horizontal motions resembling transient wall jets, which if present, could cause the drag plate to "feel" more stress.

Amongst the gravel roughness elements there are many facets of the individual particles which can potentially be acted upon by velocity vectors approaching normally to them. The flow near the tops of the roughness elements is characterised by large angular excursions in the velocity vectors (Krogstad *et al*., 1992) which increases the probability that they will interact with the roughness element surfaces in some approximation of the bluff body model. Although the turbulent environment within the roughness is different from the freestream and freestream drag coefficients are of little relevance (Finnigan and Raupach, 1986), never the less some additional form drag should be exerted on the elements. This effect, if present, should grow in proportion to the magnitude and frequency of turbulent sweep events. The evidence for increased wall bursting was seen in this research in the scaling of the standard deviation of shear stress with both roughness and velocity. Krogstad *et al*. (1992) confirmed the presence of this process with detailed quadrant analysis of the horizontal and vertical velocity components over rough surfaces.

According to Krogstad *et al*. (1992), as roughness declines, the wall bursting process begins to favour outward flow interactions that move away from the surface. Generally stated, as surfaces become smoother, the more closely they approximate the skin friction model of the *law of the wall*. This general trend was supported by the relationships found between shearing stress measured with the drag plate and indirectly measured from the wind velocity profiles. As elevational relief decreased between the test surfaces, the shear stress surplus decreased from a maximum of 59 percent for the roughest surface to a deficit of 13 percent for the smoothest gravel surface. The data generally showed a convergence towards unity as the elevational range of the surface declined.

## 6. Conclusions

The relationship between irregular surface roughness form and the shear stress developed on the surface from the applied wind force was found to be very complex. The roughness form exerted a strong influence on the magnitude, as well as the dynamic behaviour of the surface shearing stress measured with the drag plate. Over the range of wind velocities generated within the wind tunnel, the differences in $u_*$ between the test surfaces were not great and generally fell within the range of 0.3 to 1.0 m s$^{-1}$ as determined from the vertical wind velocity profiles. The real differences in the three test surfaces were manifested in the behaviour of the drag plate. The shear stress data collected with the drag plate showed very different responses for each of the test surfaces to basically the same driving force in the wind. The only possible control on these responses was the difference in surface roughness characteristics as everything else other than the slightly changing environmental conditions were held relatively constant.

The roughness effect on shear stress measured with the drag plate was explained as being a function of the changes in the turbulence activity initiated by increased roughness as well as the addition of bluff body drag forces.

## Acknowledgements

## References

Bradley, E. F.: 1968, "A Shearing Stress Meter for Micrometeorological Studies", *Quarterly Journal of the Royal Meteorological Society* **94**, 380-387.

Butterfield, G.R.: 1991, "Grain Transport in Steady and Unsteady Turbulent Air Flows", *Acta Mechanica Suppl.* **1**, 97-122.

Butterfield, G.R.: 1993, "Sand Transport Response to Fluctuating Wind Velocity", in Turbulence: Perspectives on Flow and Sediment Transport, Clifford, N.J., French, J.R. and Hardisty, J. (Eds.), John Wiley & Sons, Chichester, pp. 305-336.

Garratt, J. R.: 1980, "Surface Influence Upon Vertical Profiles in the Atmospheric Near Surface Layer", *Quart. J. Roy. Meteorol. Soc*. **106**, 803-819.

Gillies, J.A.: 1994, "*A Wind Tunnel Study of the Relationships Between Complex Surface Roughness Form, Flow Geometry and Shearing Stress*", Ph.D. Thesis, University of Guelph, 231 p.

Hardisty, J.: 1993, "Frequency Analysis of Sand Transport in a Turbulent Air Flow", in Turbulence: Perspectives on Flow and Sediment Transport, Clifford, N.J., French, J.R. and Hardisty, J. (Eds.), John Wiley & Sons, Chichester, pp. 295-304.

Huang, C.-h. and Bradford, J. M.: 1992, "Applications of a laser scanner to quantify soil microtopography", *Soil Sci. Soc. Am. Journal* 56, 1, 14-21.

Huang, C.-h., White, I., Thwaite, E. G. and Bendelli, A.: 1988, "A Noncontact Laser System for Measuring Soil Surface Topography", *Soil Science Society of America Journal* **52**, 350-355.

Iversen, J. D., Wang, W.P., Rasmussen, K.R. and Mikkelsen, H.E.: 1991, "Roughness Element Effect on Local and Universal Saltation Transport", *Acta Mechanica* (Suppl.2), 65-75.

Krogstad, P.-Å., Antonia, R.A. and Browne, L.W.B.: 1992, "Comparison Between Rough- and Smooth-wall Turbulent Boundary Layers", *J. Fluid Mechanics* **245**, 599-617.

Krumbein, W.C. and F.J. Pettijohn: 1988, Manual of Sedimentary Petrography, SEPM Reprint Series No. 13, Soc. of Economic Palaeontologists and Mineralogists, Tulsa OK, 549 p.

Lee, B. E. and Soliman, B. F.: 1977, "An Investigation of the Forces on Three Dimensional Bluff Bodies in Rough Wall Turbulent Boundary Layers", *Transactions of the ASME, Journal of Fluids Engineering*, 503-510.

Levi, E.: 1983, "Oscillatory Model for Wall-bounded Turbulence", *Journal of Engineering Mechanics* **109** (3), 728-740.

McKenna-Neuman, C. and Nickling, W.G.: 1994, "Momentum Extraction with Saltation: Implications for Experimental Evaluation of Wind Profile Parameters", *Boundary-Layer Meteorol.* **68**, 35-50.

Middleton, G.V. and Southard, J.B: 1984, "Mechanics of Sediment Movement", SEPM Short Course Number 3, SEPM, Tulsa, OK.

Mulhearn, P.J. and Finnigan, J.J.: 1978, "Turbulent Flow Over a Very Rough Random Surface", *Boundary-Layer Meteorol.* **15**, 109-132.

Nickling, W.G. and Gillies, J.A.: 1993, "Dust Emission and Transport in Mali, West Africa", *Sedimentology* **40** (5), 859-868.

Nickling, W.G. and McKenna-Neuman, C.: 1995, "Development of Deflation Lag Surfaces", *Sedimentology*, **42**, 403-414

Prandtl, L.: 1932, "Zur turbulenten Strömung in Röhren und längs Platten", *Ergebn. Aerodyn. Versuchsanst* **4**, 18-29.

Rao, K.N., Narashima, R., and Narayanan, M.A.B.: 1971, "Bursting in a Turbulent Boundary Layer", *Journal of Fluid Mechanics* **80**, 401-430.

Raupach, M.R.: 1981, "Conditional Statistics of Reynolds Stress in Rough-wall and Smooth-wall Turbulent Boundary layers", *Journal of Fluid Mechanics* **108**, 363-382.

Raupach, M.R., Antonia, R.A., and Rajagopalan, S.: 1991, "Rough-wall Turbulent Boundary Layers", *Applied Mechanics Reviews* **44** (1), 1-25.

Raupach, M.R., Coppin, P.A., and Legg, B.J: 1986, "Experiments on Scalar Dispersion within a Model Plant Canopy Part I: The Turbulence Structure", *Boundary-Layer Meteorol.* **35**, 21-52.

Raupach, M.R., Thom, A.S., and Edwards, I.: 1980, " A Wind Tunnel Study of Turbulent Flow Close to Regularly Arrayed Rough Surfaces", *Boundary-Layer Meteorol.* **18**, 373-397.

Taylor, P.A.: 1988, "Turbulent Wakes in the Atmospheric Boundary Layer", in Flow and Transport in the Natural Environment: Advances and Applications Steffen, W. L. and Denmead, O. T. (Eds.), Springer-Verlag, Berlin, 270-292.

Tippens, P.E.: 1978, Applied Physics, McGraw-Hill, Toronto, 758 p.

Williams, J.J., Butterfield, G.R., and Clark, D.G.: 1994, " Aerodynamic Entrainment Threshold: Effects of Boundary Layer Flow Conditions", *Sedimentology* **41** (2), 309-328.

Wolfe, S. A.: 1993, "*Sparse Vegetation as a Surface Control on Wind Erosion*", Ph.D. Thesis, University of Guelph, 257 p.